

RESEARCH

Open Access



# Intertumoral heterogeneity of the immune microenvironment in high grade canine mast cell tumors

K. L. Bardales<sup>1†</sup>, L. Jiang<sup>1†</sup>, E. Radaelli<sup>2</sup>, C. A. Assenmacher<sup>2</sup>, J. A. Lenz<sup>1</sup> and M. J. Atherton<sup>1,3\*</sup>

## Abstract

**Background** Canine cutaneous mast cell tumors (MCTs) are a common, yet clinically challenging tumor type given their variable biological behavior. Although patients with low grade MCTs can often be effectively managed with surgery alone, most dogs with high grade MCTs succumb to their disease despite multimodal therapy. An improved understanding of the immune tumor microenvironment (TME) may help identify novel prognostic and therapeutic targets.

**Methods** In this study, we interrogated the immune transcriptional profiles of the TME in low and high grade MCTs, and quantified intratumoral T cells. Twelve client-owned dogs with MCTs (6 Kiupel low grade with clinically benign behavior and 6 Kiupel high grade with clinically aggressive behavior) that underwent curative-intent surgery were selected. Tumor grade was confirmed by a single veterinary pathologist. RNA was extracted from all tumors followed by immune transcriptional profiling utilizing the NanoString Canine IO panel and analysis using the ROSALIND platform. T cell density was determined by immunohistochemical staining for CD3 and quantified using ImageScope software (Leica Biosystems) following digital slide capture. Lymphocytic infiltrate was further characterized in the TME of one high grade MCT using co-immunofluorescence.

**Results** Immune transcriptional profiling identified 9 differentially expressed genes between low and high grade MCTs ( $p\text{-adj} < 0.05$ ). Programmed cell death protein 1 (*PDCD1*) and inducible T-cell costimulator ligand (*ICOSLG*) gene expression were significantly higher in a subset of high grade MCTs. *ICOSLG* expression positively correlated with T cell score ( $r_s = 0.6434$ ,  $p = 0.0278$ ). Although the T cell density was not significantly different between low (mean of 76.42 CD3+ /mm<sup>2</sup>, SD 12 CD3+ /mm<sup>2</sup>) and high grade MCTs (mean of 129.1 CD3+ /mm<sup>2</sup>, SD 96.06 CD3+ /mm<sup>2</sup>), greater variation of T cell densities was observed across high grade MCTs compared to low grade ( $p = 0.0059$ ). Immunofluorescence of one high grade MCT with marked T cell infiltration revealed organized aggregates of T and B cells consistent with tertiary lymphoid structures (TLS).

**Conclusions** Our data revealed significant differences in the immune TME of low and high grade MCTs and provides rationale to further investigate potential prognostic and therapeutic roles of immune checkpoints in canine MCTs.

**Keywords** Mast cell tumor, Tumor microenvironment, Transcriptional profiling, Tumor infiltrating lymphocytes

<sup>†</sup>K. L. Bardales and L. Jiang contributed equally to this work.

\*Correspondence:

M. J. Atherton

mattath@upenn.edu

Full list of author information is available at the end of the article



## Background

Canine cutaneous mast cell tumors (MCTs) represent a very common, yet clinically challenging tumor in veterinary medicine. They account for 16–21% of all canine skin tumors, making them the most frequently diagnosed cutaneous neoplasm in dogs [1, 2]. Despite their prevalence, their biological behavior remains heterogeneous and difficult to predict [1, 3]. Some arise as slow growing solitary lesions that can be effectively cured with surgical excision alone, while others undergo rapid local and distant progression despite aggressive multimodal therapy [1, 3, 4]. Numerous factors have been identified to help guide prognostication and treatment recommendations, but histologic grade continues to be the most useful pathologic predictor for outcome [1, 3].

Over the years, multiple histologic grading schemes have been developed for MCTs, but the 3-tier system proposed by Patnaik has remained the most widely utilized [5]. Using this scheme, grades are assigned based on cellular criteria of malignancy such as mitotic count, degree of differentiation and degree of necrosis. Grade 1 (well-differentiated) tumors typically carry a favorable prognosis, while grade 3 (poorly differentiated) tumors are more likely to follow an aggressive disease course and be life-limiting. The outcomes for grade 2 tumors vary substantially with roughly 50% of patients having long-term survival and 50% succumbing to their disease within 5 years of diagnosis [5]. Since the majority of MCTs fall into the intermediate grade 2 category, Kiupel proposed a 2-tier grading system (low vs high) based on mitotic count, presence of multinucleation and degree of karyomegaly to improve concordance among pathologists and reduce the ambiguity associated with grade 2 tumors [6]. Today, it is common practice for pathologists to provide a grade using both the Patnaik and Kiupel systems as a clinical consensus of which is the most useful has not been reached [1]. Although grade confers important prognostic and therapeutic data, an incomplete understanding underlying the pathology of cutaneous MCT continues to impede clinical decision making.

While low grade MCTs can be successfully managed with surgery alone, patients with high grade MCTs frequently succumb to their disease [6]. Although high grade MCTs are usually associated with worse outcomes, a subset of patients diagnosed with these tumors may still have prolonged survival times after definitive treatment [7, 8]. Thus, there is an unmet need to better understand what drives aggressive behavior and to identify potential therapeutic targets to guide development of novel therapeutic approaches. In human oncology, interrogation of the immune tumor microenvironment (TME) has revealed prognostically relevant data for multiple tumor histotypes as well as therapeutically relevant biomarkers

[9–11]. Likewise, transcriptional analyses of the immune TME using NanoString technology has revealed transcriptional signatures implicated in the response and resistance to novel immunotherapies in preclinical murine models [12, 13]. We have leveraged this technology to interrogate the TME at a transcriptional level in canine histiocytic sarcoma [14, 15]. Currently, such data regarding the immune TME in MCTs and its correlation with clinical outcome is limited.

Immune checkpoint blockade has revolutionized the treatment of multiple human malignancies [16]. The recent conditional FDA approval of gilvetmab, the first programmed cell death protein 1 (PD-1) blocking antibody currently licensed for canine MCT and melanoma patients, holds promise for these malignancies amongst others. Recent studies utilizing immunohistochemical (IHC) analyses suggest immune modulation of the TME in high grade MCTs, characterized by increased numbers of infiltrating macrophages (Iba1+) and PD-1+ cells, as well as RANK/RANK-L signaling and upregulation of programmed death-ligand 1 (PD-L1) [17, 18]. In a separate study, Pulz et al. revealed that cancer associated fibroblasts (CAFs) were associated with high risk behavior in canine MCTs using a transcriptional approach [19]. Other groups have also investigated the TME of canine MCTs uncovering numerous transcriptional and IHC-based correlates to biologic MCT behavior [20–22]. This literature is consistent with immune modulation in the TME of canine MCTs and provides support for continued investigation of the immune microenvironment in canine MCT.

The primary objective of this pilot study was to compare the transcriptional differences in the immune TME of both low and high grade MCTs exhibiting biologically benign and aggressive behavior respectively. Following transcriptional profiling we subsequently quantified T cell infiltrates within the TME using IHC and immunofluorescence (IF). We identified nine differentially expressed genes (DEGs) between low and high grade MCT including transcripts encoding programmed cell death protein 1 (*PDCDI*) and inducible T-cell costimulator ligand (*ICOSLG*) in a subset of high grade MCTs. We also document a spectrum of T cell inflammation in the TME of canine MCTs.

## Methods

### Study population

The electronic medical record system and the diagnostic laboratory database were searched to retrospectively identify client-owned dogs that underwent surgical removal of a cutaneous MCT at the Matthew J. Ryan Veterinary Hospital, University of Pennsylvania between January 2011–August 2023. Search criteria included

the keywords: mast cell tumor or MCT. In addition to curative-intent tumor resection, inclusion in this study required: histopathologic confirmation of cutaneous MCT, treatment-naive tumors (no prior surgery, radiation, chemotherapy, or recent immunomodulatory therapy for any cause within 5 months), no overt evidence of local or distant metastatic disease at the time of diagnosis, detailed follow-up data for at least one year without recurrence for low grade tumors, date of recurrence or date of disease-related death for high grade tumors, and availability of formalin-fixed paraffin-embedded (FFPE) MCT primary tumor tissue. Cases were included if the histologic grade matched the expected biologic behavior, such that patients with low grade tumors experienced prolonged survival with no evidence of progression for at least 35 months and patients with high grade tumors experienced documented MCT disease progression within 14 months. Primary tumors that were not large enough to enable RNA extraction were excluded. If multiple primary tumors were present and we were unable to confirm which primary tumor progressed, then these tumors were also excluded. Referring veterinarians and clients were contacted to obtain any required information absent from the medical record. All tumors were graded according to the Patnaik and Kiupel grading schemes at the time of excision and then H&E tumor samples were retrospectively reviewed again by a single board-certified anatomic pathologist to confirm the grade and mitotic count in line with recommended standardization for mitotic count quantification (CAA) [23]. Additional data collected included: signalment, body weight, presenting complaint, date of diagnosis (via cytology or histopathology), tumor size, tumor location, clinicopathologic results, imaging results, date of surgery, biopsy features (histologic grade—Patnaik and Kiupel, mitotic count), type of adjuvant therapy, date of progression, date of death, or date of last contact, and comorbidities. Disease progression was defined as local recurrence or metastasis. All data in this study were obtained from samples collected in routine clinical care, including use of residual FFPE tissues and medical record review. Retrospective studies are exempt from review by the University of Pennsylvania's Institutional Animal Care and Use Committee and the Veterinary School Privately Owned Animal Protocol Committee.

#### RNA isolation and hybridization

For each tumor a slide was reviewed, and tumor margins were outlined by a single board-certified anatomic pathologist (CAA). Corresponding tumor blocks were then trimmed to remove normal tissue. 4×5um scrolls were cut and discarded from each block and a further 4 scrolls were collected into microcentrifuge tubes for

RNA extraction. RNA was isolated immediately using RNeasy FFPE Kit (Qiagen). RNA concentrations were determined using Qubit 4 Fluorometer (Thermo Fisher) and samples were stored at −80 °C. DV200 values were determined using TapeStation (Agilent) and sample loading volume was normalized to contain 100 ng RNA input for each sample using the following formula: volume to load (μL)=(100/DV200)×[RNA(ng/μL)] and diluted appropriately to a total volume of 5μL with water. The entire 5μL RNA solution was hybridized with gene specific reporter and capture probes (nCounter Canine IO panel) at 65 °C for 18 h and processed on the nCounter Prep station. Data was acquired using nCounter scanner, both systems are part of the NanoString nCounter Flex system.

#### Immunohistochemistry and immunofluorescence

For immunohistochemistry and immunofluorescence, 5 μm thick FFPE sections of each MCT were mounted on ProbeOn™ slides (Thermo Fisher Scientific). The immunostaining procedure was performed using a Leica BOND RXm automated platform combined with the Bond Polymer Refine Detection kit (Leica #DS9800). Briefly, after dewaxing and rehydration, sections were pretreated with the epitope retrieval BOND ER2 high pH buffer (Leica #AR9640) for 20 min at 98 °C. Endogenous peroxidase was inactivated with 3% H<sub>2</sub>O<sub>2</sub> for 10 min at room temperature (RT). Nonspecific tissue-antibody interactions were blocked with Leica PowerVision IHC/ISH Super Blocking solution (PV6122) for 30 min at RT. The same blocking solution also served as diluent for the primary antibody. A primary rat monoclonal antibody against CD3ε (CD3, Bio-Rad MCA1477T, clone CD3-12) was used at a concentration of 1/600 and incubated on the slides for 45 min at RT. A biotin-free polymeric IHC detection system consisting of HRP conjugated anti-rat IgG was then applied for 25 min at RT. Immunoreactivity was revealed with the diaminobenzidine (DAB) chromogen reaction. Slides were finally counterstained in hematoxylin, dehydrated in an ethanol series, cleared in xylene, and permanently mounted with a resinous mounting medium (Thermo Scientific ClearVue™ coverslip). Sections of canine lymphoid tissues were included as positive controls. Negative controls were obtained either by omission of the primary antibodies or replacement with an irrelevant isotype-matched rat monoclonal antibody. Slides were scanned using the Aperio AT2 automated slide scanner (Leica Biosystems) and visualized with the ImageScope software (Leica Biosystems). A cytoplasmic algorithm was created on ImageScope, counting CD3 positive cells. Tumor tissue was contoured prior to application of the CD3 algorithm, areas of histomorphologic necrosis were excluded from

analysis. Immunofluorescence (IF) combining CD3 (BioRad, MCA1477T, clone CD3-12), CD79b (Cell Signaling Technology, 96,024, clone D7V2F), KIT (Cell Signaling Technology, 37,805, clone D3W6Y), and 4',6'-diamidino-2-phenylindole (DAPI, Akoya Biosciences, FP1490) was also performed on a single tumor using the OPAL Automation Multiplex IHC Detection Kit (Akoya Biosciences #NEL830001KT) implemented onto a BOND Research Detection System (Leica #DS9455) according to the manufacturer instructions. For this technique, CD3, CD79b, and KIT antibodies were used at a concentration of 1/2000, 1/1000, and 1/1000, respectively. The slides were then scanned using the Aperio VERSA 200 automated slide scanner (Leica Biosystems) and visualized with the ImageScope software (Leica Biosystems).

#### Data handling and statistical analyses

Progression-free survival (PFS) times were calculated in days from date of surgery until MCT progression or death, overall survival (OS) times were calculated in days from date of surgery until death. PFS and OS and were plotted using the Kaplan–Meier (KM) product-limit estimator. Some patients were right-censored if lost to follow-up or still alive at the time of writing. KM curves were compared using the log-rank test. Correlation analyses were performed using two-tailed Spearman correlation. T cell scores and T cell densities were compared between groups using two-tailed Mann–Whitney tests. Homogeneity of variances were compared using the Fligner–Killeen test. Statistical significance was established at  $p < 0.05$ . Statistical analyses were performed using Prism v10 (GraphPad) and R v4.4.2 (R Core Team).

NanoString data were analyzed by ROSALIND (<https://rosalind.bio/>), with a HyperScale architecture developed by ROSALIND, Inc. Normalization, fold changes, and  $p$  values were calculated using criteria provided by NanoString. ROSALIND follows the nCounter Advanced Analysis protocol of dividing counts within a lane by the geometric mean of the normalizer probes from the same lane. Housekeeping probes to be used for normalization were selected based on the geNorm algorithm as implemented in the NormqPCR R library [24].  $p$  value adjustment was performed using the Benjamini–Hochberg method of estimating false discovery rates (FDR) when comparing all low and high grade MCTs. Clustering of genes for the final heatmap of differentially expressed genes was done using the PAM (Partitioning Around Medoids) method using the fpc R library (<https://cran.r-project.org/web/packages/fpc/index.html>) that takes into consideration the direction and type of all signals on a pathway, the position, role, and type of every gene, etc. Differentially expressed genes were reported when fold change was  $\geq 1.5$  or  $\leq -1.5$

and were considered statistically significant when  $p\text{-Adj} \leq 0.05$  when comparing Kiupel low to high grade MCTs. Immune cell scores were determined for each tumor using a Cell Type Profiling algorithm embedded in ROSALIND.

## Results

### Identification and description of clinically benign and aggressive MCTs

Twelve client-owned dogs with cutaneous MCTs were identified for inclusion in this study (Table 1). The median age at diagnosis was 8.5 years (range 5–13 years) and 58% of the study population was female. Five of the dogs (42%) were considered predisposed breeds, including Labrador retrievers, a boxer, a French bulldog and a pug [1, 25]. Of the 12 MCTs selected for analysis, 6 were low grade (one grade 1, five grade 2) and 6 were high grade (two grade 2, four grade 3). Most tumors were 1–3 cm in diameter (66%) with a roughly even anatomic distribution along the head/neck (25%), trunk (42%) and limbs (33%). Preoperative staging diagnostics were performed at the attending clinician's discretion. In total, 11 dogs (92%) had a CBC/Chemistry, 4 dogs (33%) had thoracic radiographs, 5 dogs (42%) had an abdominal ultrasound, and 3 dogs (25%) had regional lymph node aspirates. None of the patients had preoperative liver or spleen aspirates performed. No overt metastatic disease was documented in any dog prior to surgery. For the 6 low grade MCTs, both the median PFS and OS was 1889 days. The median PFS and OS for the 6 high grade MCTs was 184.5 days and 363.5 days respectively. PFS and OS was significantly longer for the low grade tumors (Fig. 1). Mitotic count was significantly higher in high grade tumors compared to low grade tumors (Table 1, Figure S1). Collectively, our inclusion and exclusion criteria generated two groups of MCTs with polarized outcomes. Specifically, we selected 6 histologically low grade tumors with associated benign biologic behavior to compare with 6 histologically high grade tumors with associated aggressive biologic behavior.

### Transcriptional profiling reveals significant differences between low and high grade MCTs

Across all samples, we found nine DEGs ( $p\text{-Adj} < 0.05$ ) (Fig. 2A–C). *ICOSLG*, *PDCD1*, *CDKN2C*, and *BRCA1* exhibited overall increased expression in high compared to low grade tumors, *EPSTI1*, *ESR1*, *THY1*, *ERBB2*, and *TNKS* exhibited overall decreased expression in high compared to low grade tumors (Fig. 2A–C, Table S1). Our data revealed significant transcriptional differences between the TME of low and high grade canine MCTs. This included upregulation of the tumor suppressor genes *CDKN2C* and *BRCA1* in high grade MCTs. As

**Table 1** Clinical characteristics of 12 dogs with cutaneous MCT

ID	Signalment	Kiupel grade	Patnaik grade	Mitotic count	Surgical intent	Adjuvant treatment	PFS days	OST days	Censor
MCT-1	7 YO FS pug	Low	I	3	Curative	None	1889	1889	No
MCT-2	9 YO MN Labrador	Low	II	0	Curative	None	1083	1083	Yes
MCT-3	8 YO MN Yorkshire terrier	Low	II	2	Curative	None	1273	1273	No
MCT-4	5 YO MN Labrador	Low	II	0	Curative	None	1371	1371	Yes
MCT-5	5 YO FS boxer	Low	II	0	Curative	None	1869	1869	Yes
MCT-6	6 YO FS mixed breed	Low	II	1	Curative	None	2894	2894	Yes
MCT-7	9 YO FS mixed breed	High	II	14	Curative	Vinblastine, prednisone, CCNU, toceranib, and radiation therapy	193	501	No
MCT-8	9 YO MN Yorkshire terrier	High	II	37	Curative	Vinblastine, prednisone, and toceranib	405	405	No
MCT-9	11 YO MN shiba inu	High	III	32	Curative	Vinblastine, prednisone, toceranib, CCNU, and radiation therapy	140	322	No
MCT-10	8 YO FS French bulldog	High	III	12	Curative	None	176	413	No
MCT-11	13 YO FS mixed breed	High	III	13	Curative	Vinblastine, prednisone	272	272	No
MCT-12	11 YO FS mixed breed	High	III	26	Curative	None	43	43	No

these genes encode for proteins that can activate cell cycle checkpoints we interrogated correlations of these transcripts with mitotic count and in both instance documented significant positive correlations (Figure S2) [26, 27]. Although non-biased clustering of the DEGs resulted in segregation of low and high grade tumors, we noted that *ICOSLG* and *PDCD1* were only upregulated in a subset of 3 of the high grade canine MCTs (Fig. 2B). As inducible T cell costimulator ligand (ICOSL encoded by *ICOSLG*) and programmed death cell protein 1 (PD-1 encoded by *PDCD1*) are members of T cell checkpoint axes and expression of checkpoint molecules are frequently associated with intra-tumoral T cell infiltration, we subsequently investigated T cells within the TMEs of MCT [28–30].

#### Infiltrating T cell densities are variable but not associated with MCT grade

We found a moderate, statistically significant correlation between *ICOSLG* and transcriptional T cell score (Fig. 3A), and a similar but non-significant trend between *PDCD1* and transcriptional T cell score (Fig. 3B). We found no significant differences when comparing transcriptional T cell scores (Fig. 3C) and immunohistochemical densities of CD3 labelled lymphocytes (Fig. 3D) between high (mean T cell score of 5.589 and mean IHC counts of 129.1 CD3+ /mm<sup>2</sup>) and low grade (mean T cell score of 5.569 and mean IHC counts of 76.42 CD3+ /mm<sup>2</sup>) tumors. However, high grade MCTs exhibited a trend for greater variances of

transcriptional T cell scores (SD 1.031), and significantly greater variances of IHC T cell densities (SD 96.06 CD3+ /mm<sup>2</sup>) compared to low grade MCT T cell scores (SD 0.3409) and IHC T cell densities (SD 12 CD3+ /mm<sup>2</sup>) (Fig. 3C + D) ( $p=0.1186$  for T cell scores and  $p=0.0059$  for IHC T cell densities). Analyses of other available transcriptional immune cell scores including cytotoxic cells, Th1 cells, NK CD56 dim cells and macrophages revealed no significant differences of the scores between high and low grade MCTs (Figure S3A–D). We found no significant correlations between transcriptional cytotoxic cell score, transcriptional Th1 cell score, or transcriptional macrophages score and *ICOSLG* nor *PDCD1*, however we documented significant positive correlations between *ICOSLG* and *PDCD1* with the transcriptional NK CD56 dim cell scores (Figure S4 + S5). T cells were predominantly scattered individually throughout the TME of MCTs, however IHC studies identified large coalescing clusters of CD3+ T cells in one high grade tumor (MCT-12) (Fig. 3E), and co-immunofluorescent studies revealed concentric arrangements of CD3+ T cells around CD79b+ B cells forming follicles within the tumor stroma reminiscent of tertiary lymphoid structures (TLS) (Fig. 3F). Accordingly, MCT-12 had the greatest transcript levels of *ICOSLG* and *PDCD1* (Figs. 2B and 3A + B), alongside the highest T cell score (Fig. 3C) and T cell density determined by IHC (Fig. 3D). Taken together, we found variable T cell inflammation of canine MCT TMEs and observed a broad spectrum of T cell infiltration between the TMEs of individual high grade MCTs.

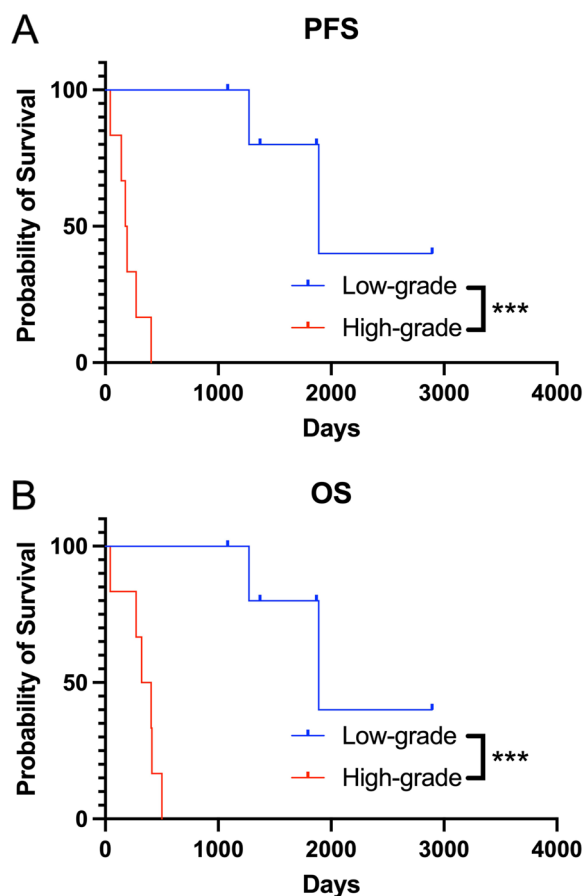


**Fig. 1** A cohort of 6 dogs with biologically benign low grade MCT and 6 dogs with biologically aggressive high grade MCT. Kaplan–Meier curves for **A.** progression-free survival and **B.** overall survival. (Curves compared using log-rank tests,  $*** p=0.0005$ .)

## Discussion

By using a combination of transcriptional and protein-based techniques, we were able to detect changes in the TME of canine cutaneous MCTs associated with benign and aggressive disease courses. Notably, whilst the TME of low grade MCTs appeared relatively homogenous both transcriptionally and at the level of T cell inflammation, there was greater variability in our cohort of high grade MCTs. Interrogating factors that modulate the immune TME in high grade MCT and ascertaining whether specific subsets of high grade MCT patients can be targeted with immune therapies are areas worthy of ongoing study.

We found upregulation of *ICOSLG* and *PDCD1* encoding for ICOSL and PD-1 respectively in three of six high grade cases. The binding of ICOSL and PD-L1/2 expressed by tumor cells or APCs to ICOS and PD-1 respectively modifies the activity of T cells bearing these cognate receptors [28, 29]. In the case of ICOS signaling,

binding of the receptor by the ligand can either lead to anti-tumor activity through stimulation of ICOS+ effector T cells or pro-tumorigenic activity by stimulating ICOS+ regulatory T cells (Tregs) [29]. This dichotomy has driven the preclinical development of therapies designed to have either agonistic or blocking activity within this checkpoint axis in cancer patients [29]. Classically, PD-1 signaling has been associated with suppression of effector T cell activity as a mechanism of peripheral tolerance, and this pathway is frequently coopted by tumors and constitutes a significant form of tumor immune evasion [28]. Blockade of the PD-1: PD-L1/2 interaction has resulted in durable clinical benefits for patients with multiple different tumor types and holds promise for canine patients following the conditional approval of gilvetmab [28]. In our study, we found a subset of high grade MCTs that exhibited increased expression of some of these checkpoint transcripts in patients that had an aggressive disease course despite undergoing curative intent therapies. It is tempting to speculate that dogs with higher *PDCD1* expression within the MCT TME may respond favorably to PD-1 blockade, however, it should be noted that in human oncology there are no biomarkers that uniformly predict the success of immune checkpoint inhibition at an individual level [31]. Nonetheless, the presence of checkpoint transcripts within some high grade MCTs does provide rationale for further investigation into the function, and potential therapeutic targeting, of immune checkpoints in canine mast cell disease. Future studies and trials should be designed in such a way as to capture patient samples enabling accurate correlative analyses to be performed and linked to tumor response data.

Other transcripts that were significantly upregulated in high grade MCTs included breast cancer gene 1 (encoded by *BRCA1*) and cyclin dependent kinase inhibitor 2C (*CDKN2C*) and at a transcriptional level both were positively correlated with mitotic count in our dataset. *BRCA1* and *CDKN2C* are tumor suppressor genes contributing to the activation of cell cycle checkpoints [26, 27]. Mutations of *BRCA1* have been implicated in the development of canine mammary tumors and loss of *CDKN2C* has been detected in canine glioma [32, 33]. Conversely increased expression of both genes have been associated with poor outcomes in specific subtypes of human lung cancers [34, 35]. We also found five transcripts that were enriched in low grade MCTs. Estrogen receptor (*ESR1*) has been previously detected in the cytosol of canine MCTs, but association with prognosis has not been substantially investigated [36]. Human epidermal growth factor receptor 2/neu (*ERBB2*) is overexpressed in other canine malignancies including osteosarcoma, however, no association with MCT and grade has been previously described [37]. Tankyrase (*TNKS*) is member

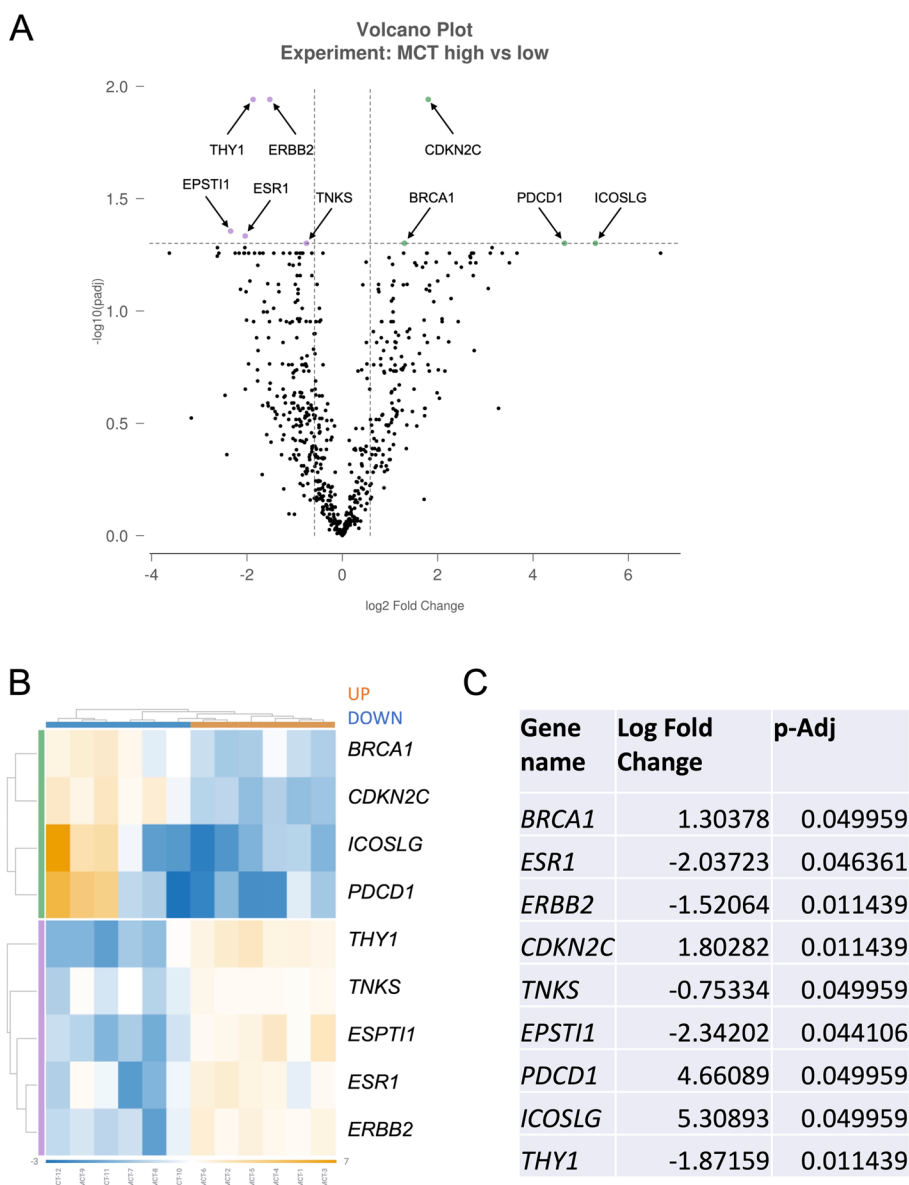


**Fig. 2** Transcriptional profiling of cutaneous MCTs. Identification of differentially expressed genes (DEGs) between low and high grade MCTs displayed in **A**. volcano plot, **B**. gene clustering depicted by heatmap, and **C**. list of log<sub>2</sub> fold changes and adjusted *p* values for DEGs. (Data derived from NanoString canine IO panel and analyzed using the ROSALIND platform, colors of the heatmap represent log<sub>2</sub> normalized gene expression after subtracting the mean on a per-gene basis with orange representing increased expression and blue representing decreased expression, the horizontal bar at the top of the heatmap collectively represents low grade tumors in orange and high grade tumors in blue, the vertical bar to the left of the heatmap collectively represents a set of genes with increased expression in high grade tumors in green corresponding to the green dots in the volcano plot and a set of genes with increased expression in low grade tumors in purple corresponding to the purple dots in the volcano plot.)

of the family of poly(adenosine diphosphate-ribose) polymerases and is involved in multiple cellular processes that are dysregulated in cancer including telomere maintenance, signal transduction, mitosis, and DNA repair [38]. Epithelial stromal interaction 1 (*EPSTI1*) has been implicated in epithelial to mesenchymal transition in

human breast cancer cells [39]. Finally, Thy-1 (*THY1*) is expressed by multiple different cell types, including various immune cells, and is also implicated in numerous processes involved in tumor development [40]. Larger and more comprehensive studies to confirm the biologic relevance of these transcriptional changes are required to

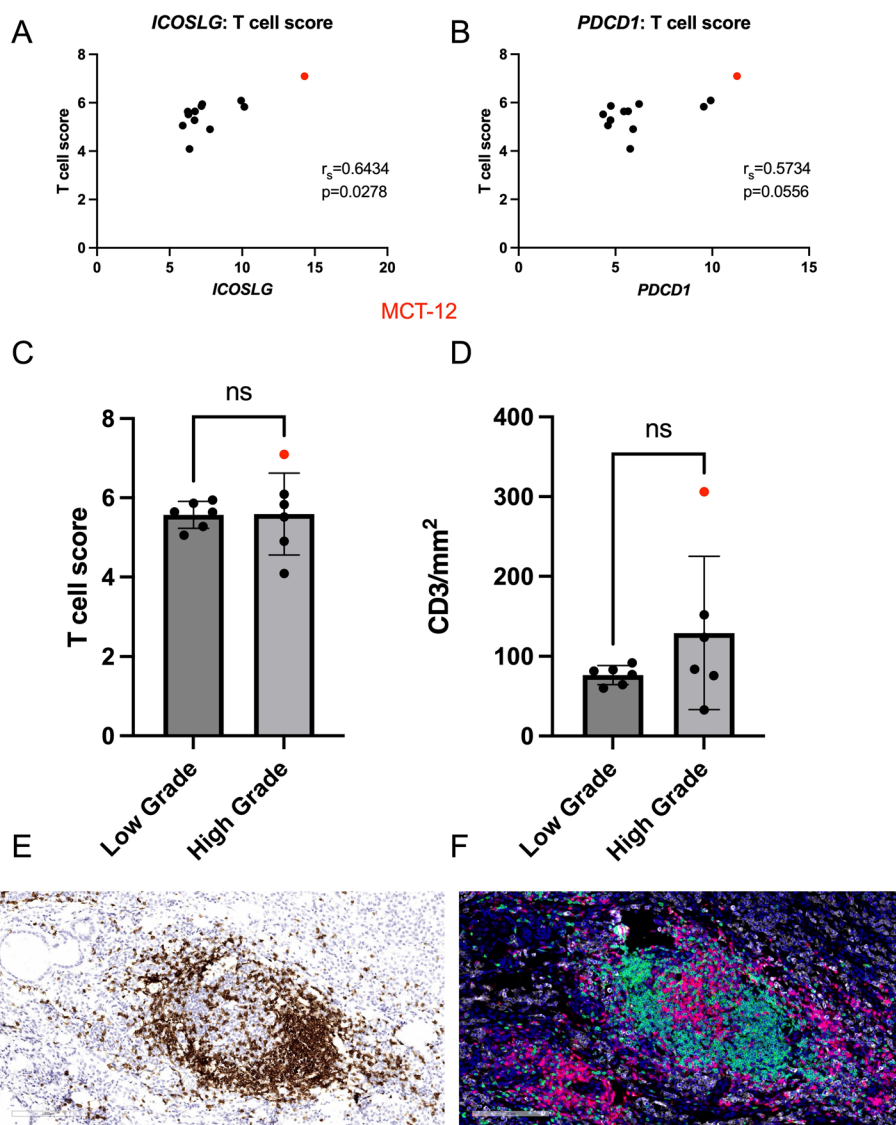


**Fig. 3** Assessment of tumor infiltrating lymphocytes in canine MCTs. Correlative analyses of transcriptional T cell score with **A.** *ICOSLG* and **B.** *PDCD1* transcripts (each dot represents an individual dog using log2 normalized expression of transcripts). Comparisons of **C.** transcriptional T cell score **D.** and density of CD3+T cells determined immunohistochemically between low and high grade MCTs (mean and standard deviations displayed). Images of lymphoid aggregates consistent with tertiary lymphoid structures within the high grade MCT-12 using **E.** immunohistochemical staining against CD3 (DAB chromogen reaction and hematoxylin counterstain) and **F.** co-immunofluorescent labelling of CD3 (green), CD79b (red), KIT (white), nuclear DAPI (blue) labelling. (Scale bars = 200  $\mu$ m. DAB- diaminobenzidine; DAPI- 4',6'-diamidino-2-phenylindole. Correlative analyses performed using two-tailed Spearman correlation Spearman rho ( $r_s$ ) and  $p$  values displayed. Comparisons between two groups performed using two-tailed Mann-Whitney tests, ns = not significant.)

make more definitive conclusions regarding their roles in canine MCTs and how they may relate to benign or aggressive disease courses.

In line with the data reported by Costa et al., we found no significant differences in transcriptional T cell scores or CD3+T cell densities between low and high grade MCT, although both this study and our work revealed greater variation of T cells within the group of high grade MCTs [17]. Factors that regulate the degree of T

cell infiltration within the TME of MCTs are yet to be defined. Future avenues for investigation would include studies of stromal barriers to T cell infiltration, as well as the potential antigenicity of individual MCTs [28, 41]. In a prior study in canine MCT, CAFs were associated with aggressive disease and this stromal component has been associated with decreased T cell infiltration within human solid cancers [19, 28, 41]. An increased tumor mutational burden (TMB) has been associated

with increased immunogenicity of tumors and, in turn, may lead to greater T cell infiltration within tumors [28]. A recent genomic study of various canine malignancies revealed that the median TMB of MCTs could be considered to represent a moderate mutational burden compared to other canine cancers, such as pulmonary adenocarcinoma with higher median TMBs and anal sac carcinomas with lower median TMBs [42]. However, as individual MCTs were found to have variable TMBs, future studies could ascertain whether higher TMBs are positively correlated with T cell infiltration in canine MCTs [42]. Correlative analyses of stromal compartments and/or TMB with T cell density may help elucidate factors that govern T cell infiltration in high grade canine MCTs.

In human oncology, TLSs are defined by centrally organized B cell follicles surrounded by T cells and resemble lymph nodes both architecturally and functionally [43]. Notably, when found within tumors, these structures confer favorable outcomes to checkpoint blockade in human patients diagnosed with various malignancies [44]. Following our IHC studies, we identified analogous structures in one of our high grade MCT cases and confirmed the concentric arrangement of T cells around B cells between neoplastic cells using co-immunofluorescence. This individual patient initially presented with a high grade, ulcerated MCT. As such, it is feasible that secondary infection and subsequent inflammation may also have contributed to the TLSs noted in this tumor [45]. Alternatively, the TLSs documented may indicate this MCT was immunogenic, and ulceration may have, in part, been secondary to the inflammation. Subsequent clinical trials using canine checkpoint blockade will determine whether the presence of TLSs in veterinary oncology patients is associated with good therapeutic responses.

This study suffered from several limitations inherent to smaller retrospective investigations such as heterogeneity in treatment regimens and lack of standardized follow-up. Thus, subsequent larger prospective clinical studies are needed to corroborate our findings and further investigate correlations of transcriptional findings with histologic and clinical variables. Following discovery of our transcriptional changes, we attempted to quantify PD-1 and ICOSL using IHC (data not shown). Given our observed correlations between checkpoint transcripts and tumor infiltrating immune cells, these IHC studies would have enabled us to discern whether these checkpoint molecules were expressed by lymphocytes or other cells within the TME, thus overcoming one of the limitations of bulk RNA profiling. However, we encountered non-specific staining for PD-1, which may reflect non-specific binding of MCT granules to antibodies as

previously documented [46]. We also unsuccessfully attempted to identify antibodies that were cross reactive to canine ICOSL for use in IHC. A lack of specific reagents to interpret canine immune markers is an issue currently facing our field, but, as comparative immunoncology becomes more established, we expect there will be a greater availability of validated antibodies [47]. Future analyses of fresh MCTs using techniques such as flow cytometry and single-cell RNA-sequencing could also be considered to more comprehensively characterize phenotypic and transcriptional profiles of neoplastic and stromal cells at the individual cell level. Finally, whilst this initial study was deliberately designed to interrogate the TME of dogs with polarized clinical outcomes, larger studies will be required to dissect the composition of the immune TME confined to Patnaik grade 2 MCTs, as these cases often pose greater challenges to clinicians when prognosticating or devising appropriate therapeutic plans.

## Conclusions

Our study revealed significant differences within the immune TME between low and high grade canine cutaneous MCTs. In our dataset, low grade MCTs displayed less heterogeneity in the immune TME compared to high grade at the transcriptional level, as well as in the degree of T cell inflammation. Within the high grade MCTs, we found three of six tumors to exhibit increased expression of *ICOSLG* and *PDCD1*. Further investigations to determine what factors regulate the composition of the immune TME in canine MCTs, and whether specific high grade MCTs are amenable to targeting by immune therapies, are indicated.

## Abbreviations

<i>BRCA1</i>	Breast cancer gene 1
CAF	Cancer associated fibroblast
<i>CDKN2C</i>	Cyclin dependent kinase inhibitor 2C
DAB	Diaminobenzidine
DAPI- 4',6'	Diamidino-2-phenylindole
DEG	Differentially expressed gene
<i>EPST11</i>	Epithelial stromal interaction 1
<i>ERBB2</i>	Human epidermal growth factor receptor 2/neu
<i>ESR1</i>	Estrogen receptor
FFPE	Formalin-fixed paraffin-embedded
IHC	Immunohistochemical
ICOS	Inducible T-cell costimulator
<i>ICOSL/ICOSLG</i>	Inducible T-cell costimulator ligand
KM	Kaplan-Meier
MCT	Mast cell tumor
OS	Overall survival
<i>PD-1/PDCD1</i>	Programmed cell death protein 1
PD-L1	Programed death-ligand 1
PFS	Progression-free survival
RT	Room temperature
TLS	Tertiary lymphoid structures
TMB	Tumor mutational burden
TME	Tumor microenvironment
<i>TNKS</i>	Tankyrase
Treg	Regulatory T cell

## Supplementary Information

The online version contains supplementary material available at <https://doi.org/10.1186/s44356-025-00020-9>.

Supplementary Material 1.

### Acknowledgements

The authors are grateful for the technical expertise of Esha Banerjee and Jillian Verrelle in the Penn Vet Comparative Pathology Core (RRID:SCR\_022438), and for statistical advice provided by Dr. Mark Oyama.

### Authors' contributions

KLB: data acquisition and analysis, data interpretation, manuscript preparation, and manuscript revision with final manuscript approval. LJ: data acquisition and analysis, data interpretation, and manuscript revision with final manuscript approval. ER: data acquisition and analysis, data interpretation, and manuscript revision with final manuscript approval. CAA: data acquisition and analysis, data interpretation, and manuscript revision with final manuscript approval. MJA: study conceptualization/design, data acquisition and analysis, data interpretation, manuscript preparation, and manuscript revision with final manuscript approval.

### Funding

Funding: NIH/NCI K08CA252619; Penn Vet Oncology Gift Fund for Resident Research; Abramson Cancer Center Support Grant (P30 CA016520); and NIH Shared Instrumentation Grant (S10 OD023465-01A1).

### Data availability

Data is available from the corresponding author upon reasonable request.

### Declarations

#### Ethics approval and consent to participate

All data in this study were obtained from samples collected in routine clinical care following informed owner consent, including use of residual FFPE tissues and medical record review. Retrospective studies are exempt from review by the University of Pennsylvania's Institutional Animal Care and Use Committee and the Veterinary School Privately Owned Animal Protocol Committee.

#### Consent for publication

Not applicable.

#### Competing interests

The authors declare no competing interests.

#### Author details

<sup>1</sup>Department of Clinical Sciences and Advanced Medicine, School of Veterinary Medicine, University of Pennsylvania, Philadelphia, PA, USA. <sup>2</sup>Department of Pathobiology, School of Veterinary Medicine, University of Pennsylvania, Philadelphia, PA, USA. <sup>3</sup>Department of Biomedical Sciences, School of Veterinary Medicine, University of Pennsylvania, Philadelphia, PA, USA.

Received: 24 October 2024 Accepted: 26 February 2025

Published online: 14 March 2025

### References

- Bellamy E, Berlato D. Canine cutaneous and subcutaneous mast cell tumours: a narrative review. *J Small Anim Pract.* 2022;63(7):497–511.
- Kiupel M, Camus M. Diagnosis and Prognosis of Canine Cutaneous Mast Cell Tumors. *Vet Clin North Am Small Anim Pract.* 2019;49(5):819–36.
- Blackwood L, Murphy S, Buracco P, De Vos JP, De Fornel-Thibaud P, Hirschberger J, et al. European consensus document on mast cell tumours in dogs and cats. *Vet Comp Oncol.* 2012;10(3):e1–29.
- Atherton MJ, Mason NJ. A bitesize introduction to canine hematologic malignancies. *Blood Adv.* 2022;bloodadvances.2021005045.
- Patnaik AK, Ehler WJ, MacEwen EG. Canine cutaneous mast cell tumor: morphologic grading and survival time in 83 dogs. *Vet Pathol.* 1984;21(5):469–74.
- Kiupel M, Webster JD, Bailey KL, Best S, DeLay J, Detrisac CJ, et al. Proposal of a 2-tier histologic grading system for canine cutaneous mast cell tumors to more accurately predict biological behavior. *Vet Pathol.* 2011;48(1):147–55.
- Chalfon C, Sabattini S, Finotello R, Faroni E, Guerra D, Pisoni L, et al. Lymphadenectomy improves outcome in dogs with resected Kiupel high-grade cutaneous mast cell tumours and overtly metastatic regional lymph nodes. *J Small Anim Pract.* 2022;63(9):661–9.
- Moore AS, Frimberger AE, Taylor D, Sullivan N. Retrospective outcome evaluation for dogs with surgically excised, solitary Kiupel high-grade, cutaneous mast cell tumours. *Vet Comp Oncol.* 2020;18(3):402–8.
- Taube JM, Galon J, Sholl LM, Rodig SJ, Cottrell TR, Giraldo NA, et al. Implications of the tumor immune microenvironment for staging and therapeutics. *Mod Pathol.* 2018;31(2):214–34.
- Taube JM, Klein A, Brahmer JR, Xu H, Pan X, Kim JH, et al. Association of PD-1, PD-1 ligands, and other features of the tumor immune microenvironment with response to anti-PD-1 therapy. *Clin Cancer Res.* 2014;20(19):5064–74.
- Anderson NM, Simon MC. Tumor Microenvironment. *Curr Biol.* 2020;30(16):R921–5.
- Atherton MJ, Stephenson KB, Pol J, Wang F, Lefebvre C, Stojdl DF, et al. Customized Viral Immunotherapy for HPV-Associated Cancer. *Cancer Immunol Res.* 2017;5(10):847–59.
- Atherton MJ, Stephenson KB, Tzelepis F, Bakhshinyan D, Nikota JK, Son HH, et al. Transforming the prostatic tumor microenvironment with oncolytic virotherapy. *Oncoimmunology.* 2018;7(7): e1445459.
- Lenz JA, Assenmacher CA, Costa V, Louka K, Rau S, Keuler NS, et al. Increased tumor-infiltrating lymphocyte density is associated with favorable outcomes in a comparative study of canine histiocytic sarcoma. *Cancer Immunol Immunother.* 2022;71(4):807–18.
- Lenz JA, Peng B, Assenmacher C, King A, Zhang PJ, Maki RG, et al. Identification of immune suppressor candidates utilizing comparative transcriptional profiling in histiocytic sarcoma. *Cancer Immunol Immunother.* 2025;74(2):61.
- Korman AJ, Garrett-Thomson SC, Lonberg N. The foundations of immune checkpoint blockade and the ipilimumab approval decennial. *Nat Rev Drug Discov.* 2022;21(7):509–28.
- Costa VR, Soileau AM, Liu CC, Moeller CE, Carossino M, Langohr IM, et al. Exploring the Association of Intratumoral Immune Cell Infiltrates with Histopathologic Grade in Canine Mast Cell Tumors. *Res Vet Sci.* 2022;147:83–91.
- Talavera Guillén NC, Barboza de Nardi A, Noleto de Paiva F, Dias QC, Pinheiro Fantinatti A, Fávoro WJ. Clinical Implications of Immune Checkpoints and the RANK/RANK-L Signaling Pathway in High-Grade Canine Mast Cell Tumors. *Animals (Basel).* 2023;13(12):1888.
- Pulz LH, Barra CN, Alexandre PA, Huete GC, Cadrobbi KG, Nishiya AT, et al. Identification of two molecular subtypes in canine mast cell tumours through gene expression profiling. *PLoS ONE.* 2019;14(6): e0217343.
- Bowlt Blacklock K, Birand Z, Biasoli D, Fineberg E, Murphy S, Flack D, et al. Identification of molecular genetic contributors to canine cutaneous mast cell tumour metastasis by global gene expression analysis. *PLoS ONE.* 2018;13(12): e0208026.
- Giantin M, Granato A, Baratto C, Marconato L, Vascellari M, Morello EM, et al. Global gene expression analysis of canine cutaneous mast cell tumor: could molecular profiling be useful for subtype classification and prognostication? *PLoS ONE.* 2014;9(4): e95481.
- Bertola L, Pellizzoni B, Giudice C, Grieco V, Ferrari R, Chiti LE, et al. Tumor-associated macrophages and tumor-infiltrating lymphocytes in canine cutaneous and subcutaneous mast cell tumors. *Vet Pathol.* 2024;61(6):882–95.
- Meuten DJ, Moore FM, George JW. Mitotic Count and the Field of View Area: Time to Standardize. *Vet Pathol.* 2016;53(1):7–9.
- Perkins JR, Dawes JM, McMahon SB, Bennett DLH, Orengo C, Kohl M. ReadqPCR and NormqPCR: R packages for the reading, quality checking and normalisation of RT-qPCR quantification cycle (Cq) data. *BMC Genomics.* 2012;13:296.
- Śmiech A, Łopuszyński W, Ślaska B, Bulak K, Jasik A. Occurrence and Distribution of Canine Cutaneous Mast Cell Tumour Characteristics Among Predisposed Breeds. *J Vet Res.* 2019;63(1):141–8.

26. Wu J, Lu LY, Yu X. The role of BRCA1 in DNA damage response. *Protein Cell*. 2010;1(2):117–23.
27. Solomon DA, Kim JS, Jenkins S, Ransom H, Huang M, Coppa N, et al. Identification of p18 INK4c as a tumor suppressor gene in glioblastoma multiforme. *Cancer Res*. 2008;68(8):2564–9.
28. Binnewies M, Roberts EW, Kersten K, Chan V, Fearon DF, Merad M, et al. Understanding the tumor immune microenvironment (TIME) for effective therapy. *Nat Med*. 2018;24(5):541–50.
29. Solinas C, Gu-Trantien C, Willard-Gallo K. The rationale behind targeting the ICOS-ICOS ligand costimulatory pathway in cancer immunotherapy. *ESMO Open*. 2020;5(1): e000544.
30. Wu B, Zhang B, Li B, Wu H, Jiang M. Cold and hot tumors: from molecular mechanisms to targeted therapy. *Signal Transduct Target Ther*. 2024;9(1):274.
31. Li H, van der Merwe PA, Sivakumar S. Biomarkers of response to PD-1 pathway blockade. *Br J Cancer*. 2022;126(12):1663–75.
32. Rivera P, Melin M, Biagi T, Fall T, Häggström J, Lindblad-Toh K, et al. Mammary tumor development in dogs is associated with BRCA1 and BRCA2. *Cancer Res*. 2009;69(22):8770–4.
33. Dickinson PJ, York D, Higgins RJ, LeCouteur RA, Joshi N, Bannasch D. Chromosomal Aberrations in Canine Gliomas Define Candidate Genes and Common Pathways in Dogs and Humans. *J Neuropathol Exp Neurol*. 2016;75(7):700–10.
34. Li GS, Chen G, Liu J, Tang D, Zheng JH, Luo J, et al. Clinical significance of cyclin-dependent kinase inhibitor 2C expression in cancers: from small cell lung carcinoma to pan-cancers. *BMC Pulm Med*. 2022;22:246.
35. Guo F, Li C, Liu S, Li Z, Zhai J, Wang Z, et al. High BRCA1 expression is an independent prognostic biomarker in LUAD and correlates with immune infiltration. *Cancer Innov*. 2023;2(2):91–5.
36. Elling H, Ungemach FR. Sexual hormone receptors in canine mast cell tumour cytosol. *J Comp Pathol*. 1982;92(4):629–30.
37. Flint AF, U'Ren L, Legare ME, Withrow SJ, Dernel W, Hanneman WH. Overexpression of the erbB-2 proto-oncogene in canine osteosarcoma cell lines and tumors. *Vet Pathol*. 2004;41(3):291–6.
38. Yu M, Yang Y, Sykes M, Wang S. Small-Molecule Inhibitors of Tankyrases as Prospective Therapeutics for Cancer. *J Med Chem*. 2022;65(7):5244–73.
39. de Neergaard M, Kim J, Villadsen R, Fridriksdottir AJ, Rank F, Timmermans-Wielenga V, et al. Epithelial-Stromal Interaction 1 (EPSTI1) Substitutes for Peritumoral Fibroblasts in the Tumor Microenvironment. *Am J Pathol*. 2010;176(3):1229–40.
40. Yang J, Zhan XZ, Malola J, Li ZY, Pawar JS, Zhang HT, et al. The multiple roles of Thy-1 in cell differentiation and regeneration. *Differentiation*. 2020;113:38–48.
41. Joyce JA, Fearon DT. T cell exclusion, immune privilege, and the tumor microenvironment. *Science*. 2015;348(6230):74–80.
42. Rodrigues L, Watson J, Feng Y, Lewis B, Harvey G, Post G, et al. Shared hotspot mutations in oncogenes position dogs as an unparalleled comparative model for precision therapeutics. *Sci Rep*. 2023;13(1):10935.
43. Munoz-Erazo L, Rhodes JL, Marion VC, Kemp RA. Tertiary lymphoid structures in cancer – considerations for patient prognosis. *Cell Mol Immunol*. 2020;17(6):570–5.
44. Vanhersecke L, Brunet M, Guégan JP, Rey C, Bougouin A, Cousin S, et al. Mature tertiary lymphoid structures predict immune checkpoint inhibitor efficacy in solid tumors independently of PD-L1 expression. *Nat Cancer*. 2021;2(8):794–802.
45. Neyt K, Perros F, GeurtsvanKessel CH, Hammad H, Lambrecht BN. Tertiary lymphoid organs in infection and autoimmunity. *Trends Immunol*. 2012;33(6):297–305.
46. Ruck P, Horny HP, Kaiserling E. Immunoreactivity of human tissue mast cells: nonspecific binding of primary antibodies against regulatory peptides by ionic linkage. *J Histochem Cytochem*. 1990;38(6):859–67.
47. Rotolo A, Atherton MJ. Applications and Opportunities for Immune Cell CAR Engineering in Comparative Oncology. *Clin Cancer Res*. 2024;30(11):2359–69.

## Publisher's Note

Springer Nature remains neutral with regard to jurisdictional claims in published maps and institutional affiliations.